Egyptian Journal of Basic and Applied Sciences 5 (2018) 171–182

HOSTED BY

Contents lists available at ScienceDirect

Egyptian Journal of Basic and Applied Sciences

journal homepage: www.elsevier.com/locate/ejbas

Full Length Article

Microwave-assisted spent black tea leaves as cost-effective and powerful green adsorbent for the efficient removal of Eriochrome black T from aqueous solutions

Ayub Khan [a,b], Xiangke Wang [a], Kashif Gul [b], Fazli Khuda [c], Zaynab Aly [d], A.M. Elseman [a,e,*]

[a] College of Environmental Science and Engineering, North China Electric Power University, Beijing 102206, PR China
[b] Institute of Chemical Sciences University of Peshawar, Peshawar, Khyber Pakhtunkhwa 25120, Pakistan
[c] Department of Pharmacy, University of Peshawar, Peshawar, Khyber Pakhtunkhwa 25120, Pakistan
[d] Australian Nuclear Science and Technology Organisation, Lucas Heights, Sydney, Australia
[e] Electronic and Magnetic Materials Department, Advanced Material Division, Central Metallurgical Research and Development Institute (CMRDI), P.O. Box 87, Helwan, 11745 Cairo, Egypt

ARTICLE INFO

Article history:
Received 1 October 2017
Received in revised form 17 February 2018
Accepted 1 April 2018
Available online 10 April 2018

Keywords:
Microwave-assisted spent black tea leaves
Eriochrome black T
Adsorption
Thermodynamic parameters
Interaction mechanism

ABSTRACT

In this work, microwave-assisted spent black tea leaves (MASTL) were used as effective low-cost green adsorbents for the removal of Eriochrome Black T (EBT) from aqueous solutions and adequately characterized. The pH_{pzc} of MASTL was found to be 4.6. The experimental conditions, such as pH, contact time, temperature, adsorbent dose and EBT concentration, were optimized to evaluate the interaction of EBT with MASTL. The adsorption isotherms were simulated by Langmuir, Freundlich, Temkin and Dubinin-Radushkevich models. The results showed that the Langmuir model best fitted the adsorption data. The monolayer adsorption capacity was calculated to be 242.72 mg/g at 25 °C. The thermodynamic data calculated from the temperature-dependent adsorption isotherms indicated that the adsorption process was spontaneous, endothermic and physicochemical in nature. The results revealed that the MASTL could be used as low-cost green adsorbents for the efficient removal of EBT from aqueous solutions in environmental pollution clean-up.

1. Introduction

Environmental pollution is one of the major problems that the modern society faces today. Textile dyeing comprises a major part of the industries and contaminates large volume of water with dyes during different steps of dyeing and finishing processes. The other industries which use dyes in various processes include pulp mills, cosmetics, paper, printing, food and leather industries [1]. It is reported that various industries worldwide produce 7.0×10^5 tonnes of 10,000 different types of dyes on annual basis. About 1–15% of these dyes are lost as effluents during the dyeing process [2]. Dyes are synthetic colouring substances of the organic origin and are responsible both for surface and groundwater pollution [3], which can cause carcinogenic and mutagenic effects [4]. Some of the synthetic dyes are resistant to natural biodegradation and can be very dangerous for the aquatic life. They can restrict the photosynthetic activities in aquatic plants by blocking sunlight. This condition may reduce the re-oxygenation of water, which affects the normal growth of aquatic animals [5].

About 70% of the worldwide synthetic dyes consumed by dyeing industries are composed of azo dyes. A reactive azo dye has one or more azo groups (-N=N-), which act as chromophore in the molecular structure [6]. In addition, the compounds containing the azo group, represent the largest group of synthetic dyes and are difficult to degrade even at low concentrations, because they are very resistant to light, heat, chemicals and microbial attacks [7]. Therefore, the removal of such synthetic dyes have become very important before the waste industrial effluents released to the environmental water. Many attempts have been made for the removal of dyes from wastewaters using the commonly used processes including photocatalytic degradation [8], photo-Fenton reaction [9], biodegradation [10], solvent extraction, coagulation, precipitation, membrane filtration and advanced oxidation process [11,12]. Although good results were achieved with these methods, they were not free of shortcomings. The most important of which was the exhausting preparation of the materials and the difficult operation of the process. Similarly, secondary pollutants such as

* Corresponding author at: College of Environmental Science and Engineering, North China Electric Power University, Beijing 102206, PR China.
E-mail addresses: amourtada@ncepu.edu.cn, ahmedmourtada5555@yahoo.com (A.M. Elseman).

https://doi.org/10.1016/j.ejbas.2018.04.002
2314-808X/

various oxidative intermediates may produce during the photocatalytic degradation and oxidative processes, which are much toxic than their parent compounds. On the other hand, the adsorption techniques [13,14] are more simple and easy to conduct and can be applied on large scale. A number of adsorbents such as magnetite/pectin and magnetite/silica/pectin hybrid nanocomposites [15], activated carbon [16], anionic layer double hydroxide [17] and $NiFe_2O_4$ magnetic nanoparticles [18] have been applied for the removal of EBT from aqueous solutions. However, these adsorbents were expensive and difficult to synthesize. The scientists were therefore moved to produce cost-effective and eco-friendly adsorbents.

Plant materials are safer and can be prepared easily as time and cost-effective green adsorbents for the removal of a variety of pollutants. For example, the stem and leaves of *Scolymus hispanicus* L plant [2], eucalyptus bark [13] and maize stem tissue [19] were used as green adsorbents for the removal of EBT from aqueous solutions. In the same way, we selected spent tea leaves as low-cost green adsorbent for the efficient removal of EBT from aqueous solutions. Tea is one of the plant materials, which is basically the dried and processed leaves of an evergreen shrub, called *Camellia sinensis* [20]. The insoluble cell wall of tea leaves is mostly made up of cellulose and hemicelluloses, condensed tannins, lignin and structural proteins. As these constituents possess various functional groups, the tea leaves should have good potentials for dyes removal from aqueous solutions. The groups in lignin, tannin or other phenolic compounds which are responsible for adsorption are mainly carboxylate, aromatic carboxylate, phenolic hydroxyl and oxyl groups [21]. Due to these properties, tea wastes have been extensively used for the removal of dyes. Hameed et al. used spent tea leaves (STL) for the removal of cationic dye (methylene blue) from aqueous solutions and achieved excellent results [22]. However, 3.5 g/L of the adsorbent was needed to achieve maximum adsorption of the dye. Panneerselvam et al. impregnated STL with Fe_3O_4 and applied for the removal of heavy metal ions such as nickel [21]. The results showed that STL had low adsorption ability for heavy metals and only 83.3 mg/g of nickel was removed with 12.0 g/L of the adsorbent. STL showed high adsorption rate for certain dyes such as astrazon red 6B and adsorption reached equilibrium state after 90 min [23]. Similarly, STL was applied for the efficient removal of basic yellow-2 and acid orange-7 from aqueous solutions [24]. All these authors has used STL without any treatment.

Herein, we treated STL with H_2SO_4 followed by the microwave treatment, which not only increased its surface area but also the adsorption capacity. The MASTL was characterized with SEM and FT-IR, which helped to understand the adsorption mechanism. Excellent adsorption results were obtained with small amount of MASTL (1.0 g/L). The experimental conditions were optimized in terms of pH, temperature, contact time and adsorbent dose to achieve maximum adsorption results. The specific objective of this study was to explore the feasibility of utilization of microwave-activated STL as a nonconventional low-cost green adsorbent for the removal of EBT from aqueous solutions.

2. Materials and methods

2.1. Materials

The analytical grade anionic azo dye, Eriochrome black T (EBT), was purchased from Sinopharm Chemical Regent Co., Ltd. (Beijing, China), and used without further purification. HNO_3 and NaOH were used in the experiment and all the solutions were prepared in Milli-Q water (18.25 $M\Omega.cm^{-1}$). EBT was chosen in this study because of its known strong adsorption ability towards the solid particles.

2.2. Preparation of spent tea leaves

Sufficient amount of spent tea leaves (STL) were collected from a local tea restaurant in Charsadda, Khyber Pakhtunkhwa, Pakistan. Prior to its use, the as-collected STL (50 g) was boiled repeatedly in tap water followed by boiling in 25% ethanol three times to remove all the colour. After stirring for 10 min in 30% aqueous solution of H_2SO_4 at 100 °C, the STL dispersion was filtered and the obtained mass was subjected to microwave irradiations for 3 min at 600 W under N_2 atmosphere. The overheating in the sample was avoided by stopping the microwave oven for 5 s after every 30 s. The same treatment was repeated till dryness. After cooling to room temperature, the microwave-assisted spent black tea leaves (MASTL) were washed with Milli-Q water and 0.1 mol/L $NaHCO_3$ till to the neutral pH and finally filtered and dried in diffused sunlight for 3 days. Then it was ground to fine powder with the help of a high speed fruit blender and sieved through a micro mesh of 0.5–1.0 mm and stored in a dry and clean plastic bag.

2.3. Characterization of MASTL

The MASTL was characterized by FEI Quanta 200 FEG SEM at the energy of 15 kV. Fourier transformed infrared spectroscopy (FT-IR) was measured on a Nicolet Magana-IR 750 spectrometer at room temperature. The Brunauer-Emmett-Teller (BET) isotherm was achieved with an adsorption instrument (TriStar, Micromeritics Company, USA). The pH_{pzc} value of MASTL was determined according to a reported method [25].

2.4. Batch adsorption experiments

EBT (120 mg/L) and MASTL (6.0 g/L) were transferred to a series of polyethylene test tubes and diluted with Milli-Q water to achieve the desired concentrations. The negligible volume of 0.01 or 0.1 mol/L HNO_3 and/or NaOH were used to adjust the pH. The variances in pH before and after the adsorption experiments were kept below 0.1. The test tubes were shaken in a thermostatic shaker (BLaboratory ZQPL-200) for 24 h to achieve the adsorption equilibrium. Samples were then centrifuged at 5000 rpm for 5 min to separate the solid phase from the liquid phase. The EBT concentration was determined in the supernatant using a UV-vis spectrophotometer (Model SP-3000 plus, Optima, Tokyo, Japan) at the wavelength of 518 nm. Eq. (1) was used to calculate the amount of EBT adsorbed onto MASTL:

$$q_e = \frac{(C_o - C_e)V}{m} \quad (1)$$

where C_o and C_e (mg/L) are respectively the initial and equilibrium liquid-phase concentrations of EBT. V is the total solution volume and m is the dry mass of the adsorbent. The percent adsorption was calculated from Eq. (2):

$$Removal\ (\%) = \frac{C_o - C_e}{C_o} \times 100 \quad (2)$$

All the experimental data were taken as the average of the duplicate experiments with 5% relative errors. The procedures of kinetic and isotherm experiments were basically identical to those of equilibrium tests. In the kinetic experiments, the aqueous samples were taken at pre-set time intervals and the concentrations of EBT were measured in the same way.

3. Results and discussion

3.1. Characterization

The morphology and microstructure of MASTL was evidenced with SEM. Fig. 1 gives the SEM images of MASTL before and after

the EBT adsorption. Fig. 1A showed that before the adsorption of dye, the MASTL surface was composed of a rough and regularly arranged layered morphology with spaces in between them, which were useful for the adsorption of dye. It can be clearly seen from Fig. 1B that after EBT adsorption, the dye molecules occupied the available pores and resulted in a more dispersed and irregular mass.

The FT-IR spectrum (Fig. 1C) shows that MASTL had a number of functional groups. The broad band at 3402 cm^{-1} corresponded to the bonded –OH groups. The peaks at 2923 and 2853 cm^{-1} were due to the -C—H stretching of the alkane functional groups. Similarly, the band around 1655 cm^{-1} could be assigned to the -C═O stretching vibration of the alkene and aromatic functionality. The other peaks were found for secondary amine at 1533 cm^{-1} and N—H bending at 1455 cm^{-1}. The C—H or $-CH_3$ bending was found at 1342 cm^{-1} whereas the $-SO_3$ stretching was located at 1237 cm^{-1}. The two bands at 1146 and 1036 cm^{-1} were assigned to C-O and C═O groups, respectively [26–28]. To obtain the specific

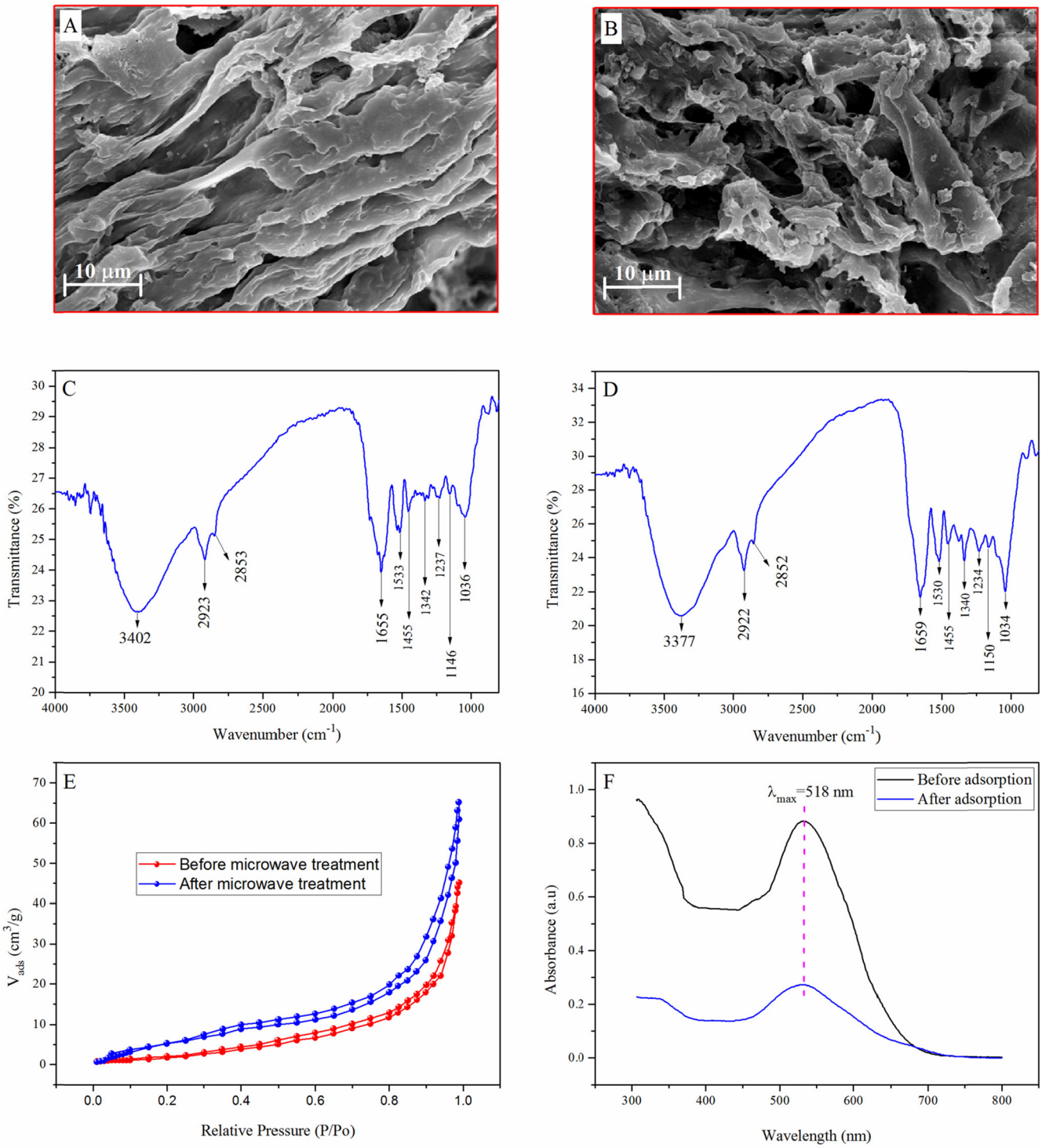

Fig. 1. SEM images of MASTL before (A) and after (B) the adsorption of dye; FT-IR spectra of MASTL before (C) and after (D) the adsorption of dye; typical N_2 adsorption-desorption isotherm of MASTL (E) and UV spectra before and after the adsorption of dye onto MASTL (F).

surface area, N_2 adsorption-desorption isotherms (Fig. 1E) were measured via a multi-point BET method. The specific surface area of STL was 25.2 m^2/g while that of MASTL was calculated to be 42.3 m^2/g. It was two times higher than that of eucalyptus bark (20.47 m^2/g), which was used for the removal of EBT from aqueous solutions [13]. The high surface area of MASTL was beneficial for the effective removal of EBT from aqueous solutions. Fig. 1F gives the UV spectra before and after the adsorption of EBT, which shows that MASTL has excellent adsorption properties towards EBT.

3.2. pH_{pzc} of MASTL

The point of zero charge (pH_{pzc}) of MASTL was determined according to the reported method [25] with some modifications. Typically, 6.0 mL of Milli-Q water was taken in a series of 10.0 mL polyethylene test tubes and the initial pH was set in the range of 2.0–9.0, with negligible volume of 0.1 mol/L HNO_3 or NaOH. Then, exactly 0.006 g of MASTL was added to each tube. The tubes were placed in a thermostatic shaker at 25 °C and agitated at 150 rpm in dark. After 24 h, the final pH in each tube was determined. The difference in the initial and final pH ($\Delta pH = pH_{initial} - pH_{final}$) was plotted against the initial pH values (Fig. 2A). The pH_{pzc} was calculated from the point where it crossed the $\Delta pH = 0$ [29], and was found to be 4.6.

3.3. Effect of solution pH

Generally, pH plays an important role in the adsorption of dyes onto suspended particles. The pH affects both the surface charge of the adsorbent and the degree of ionization of different pollutants due to the protonation-deprotonation reactions of the active functional groups. The effect of solution pH on the adsorption of EBT was studied in the range of 2.0–9.0 at 25 °C and the results were shown in Fig. 2B. The adsorption of EBT was strongly pH dependent and the highest adsorption was found at pH 2.0. At $pH < pH_{pzc}$, the surface of MASTL was positively charged due to the protonation reaction of phenolic hydroxyl groups, which promoted its reaction with anionic EBT through electrostatic interactions. Similar results were also found for the adsorption of EBT on magnetite/pectin and magnetite/silica/pectin hybrid nanocomposites [15]. A continuous decrease in the dye adsorption was found with the increase of pH, and the lowest dye adsorption (1.60–0.74 mg/g) was recorded at

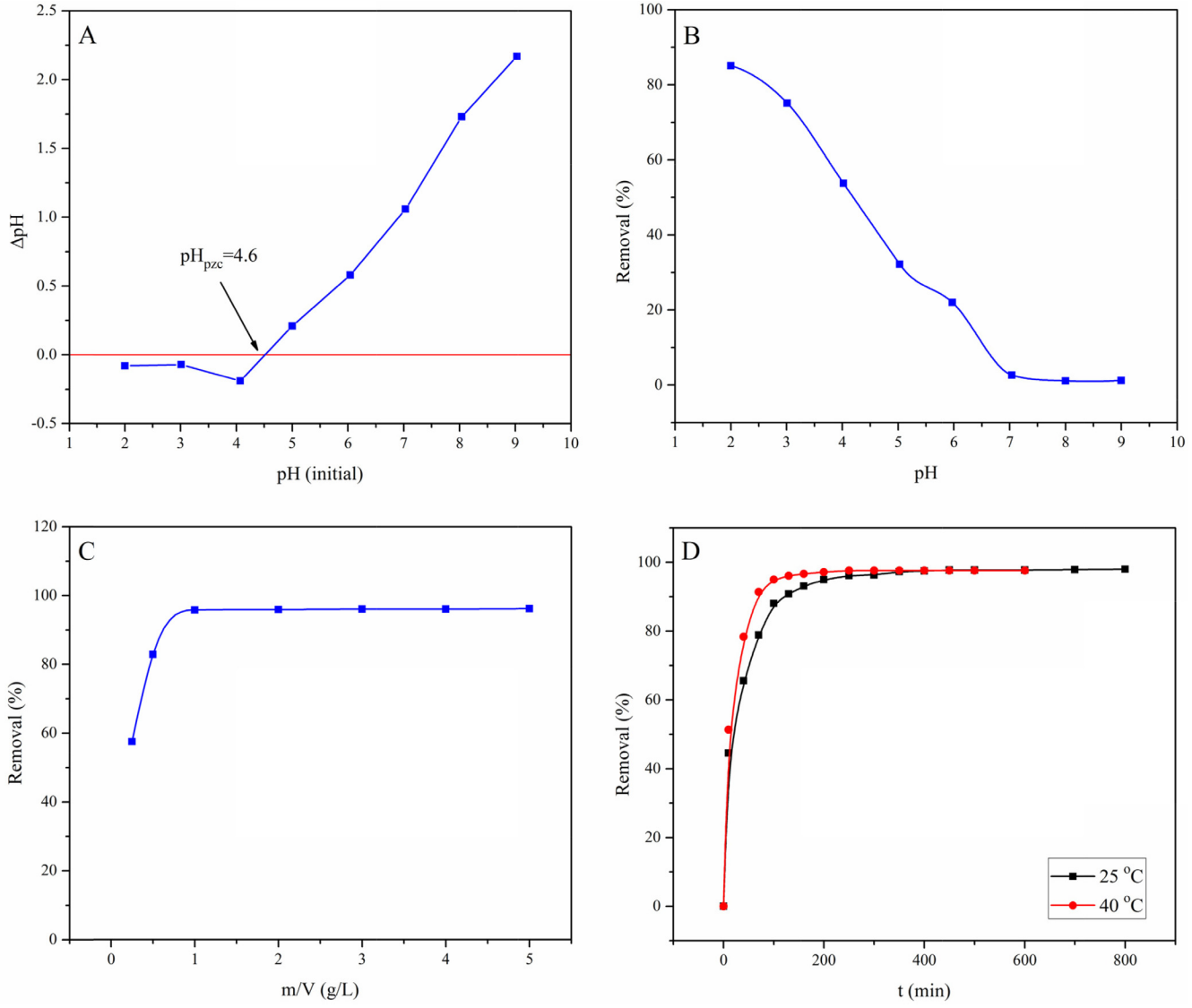

Fig. 2. Point of zero charge of MASTL (A) and the effect of the solution pH (B), at m/V = 1.0 g/L, $C[EBT]_{initial}$ = 60 mg/L, t = 24 h, and T = 25 °C; the effect of solid content (C), at pH = 2.0, $C[EBT]_{initial}$ = 60 mg/L, t = 24 h, and T = 25 °C; the effect of contact time (D), at pH = 2.0, m/V = 1.0 g/L, $C[EBT]_{initial}$ = 60 mg/L, and T = 25 °C.

pH 7.0–9.0. With the increase of pH, the positive surface charge density of MASTL decreased, which resulted in weakening of its interactions with EBT. Similarly, at pH > pH_{pzc}, the MASTL surface was negative and high electrostatic repulsions with EBT lead to a very low adsorption. Therefore, the equilibrium adsorption (q_e) decreased from 51.03 to 0.74 mg/g with the increase of pH from 2.0 to 9.0. The electrostatic attractions suggested the chemisorption of EBT onto MASTL.

3.4. Effect of adsorbent dose

Fig. 2C shows the effect of MASTL dose on the adsorption of EBT. It was observed that the removal of EBT increased from 57.6 to 95.8% with the increase of MASTL dose from 0.25 to 5.0 g/L. This is because the increase in number of adsorption sites was proportional to the number of the MASTL particles. The maximum adsorption of EBT was observed at 1.0 g/L of MASTL and was used in rest of the experiments.

3.5. Effect of contact time

Fig. 2D represents the effect of contact time on the adsorption of EBT onto MASTL at 25 and 40 °C. At 25 °C, the adsorption of EBT was rapid in the first 100 min of contact time and then slowed down till it reached the equilibrium state in about 250 min. However, this time reduced to 160 min by increasing the temperature to 40 °C. This revealed that the EBT adsorption onto MASTL was endothermic. The high initial adsorption rate of EBT was due to the availability of free adsorption sites on the adsorbent's surface. However, with the passage of time the number of available adsorption sites decreased as they were occupied by more and more pollutant molecules or ions. That is why the adsorption rate became constant at equilibrium when there was no or very few sites available for adsorption [18].

3.6. Effect of temperature and EBT concentration

Fig. 3 shows the effect of initial concentration and temperature on the adsorption profile of EBT. Fig. 3A shows that the adsorption increased with the increase of temperature from 25 to 60 °C, which may be due to the high kinetic energy of EBT molecules at high temperature. High temperature also lead to more powerful collision of EBT with MASTL and the approach of EBT molecules to the MASTL surface became easier. Similarly, it can be seen that the adsorption of EBT increased with the increase of its concentration (Fig. 3B). Furthermore, the high initial concentration provided a significant driving force to overcome all the mass transfer resistances between the EBT molecules and the adsorbent's surface. Thus the adsorption process was enhanced at high initial concentration of EBT. However, the percent adsorption decreased from 92.8 to 71.8% as the EBT concentration was increased from 10 to 400 mg/L.

3.7. Isotherm analysis

The isotherm study was important in determining the chemistry as well as the homogeneity or heterogeneity of the adsorption process. Generally, the adsorption isotherms are empirical relationships which describe the extent of adsorption as well as its mechanism. Herein, Langmuir, Freundlich, Temkin and Dubinin-Radushkevich models were applied to evaluate the equilibrium isotherm study of EBT onto MASTL.

The Langmuir isotherm theory suggests a monolayer coverage of the adsorbate over a homogenous adsorbent surface. Once a site is occupied by a molecule, no further adsorption can take place at that site. The Langmuir isotherm has been used successfully to describe the adsorption of EBT onto natural [19] and synthetic adsorbents [18]. In nonlinear form the Langmuir isotherm can be written as:

$$q_e = \frac{q_m b C_e}{1 + b C_e} \tag{3}$$

However, the linear form is more convenient to evaluate the adsorption data, which can be expressed as:

$$\frac{C_e}{q_e} = \frac{1}{q_m b} + \frac{C_e}{q_m} \tag{4}$$

where q_e (mg/g) is the amount of the pollutant adsorbed per unit mass of the adsorbent at equilibrium, C_e (mg/L) is the equilibrium concentration of the pollutant in solution, q_m (mg/g) is the maximum adsorption at complete monolayer coverage, and the parameter b (L/mg) is the sorption enthalpy constant. Fig. 4A represents

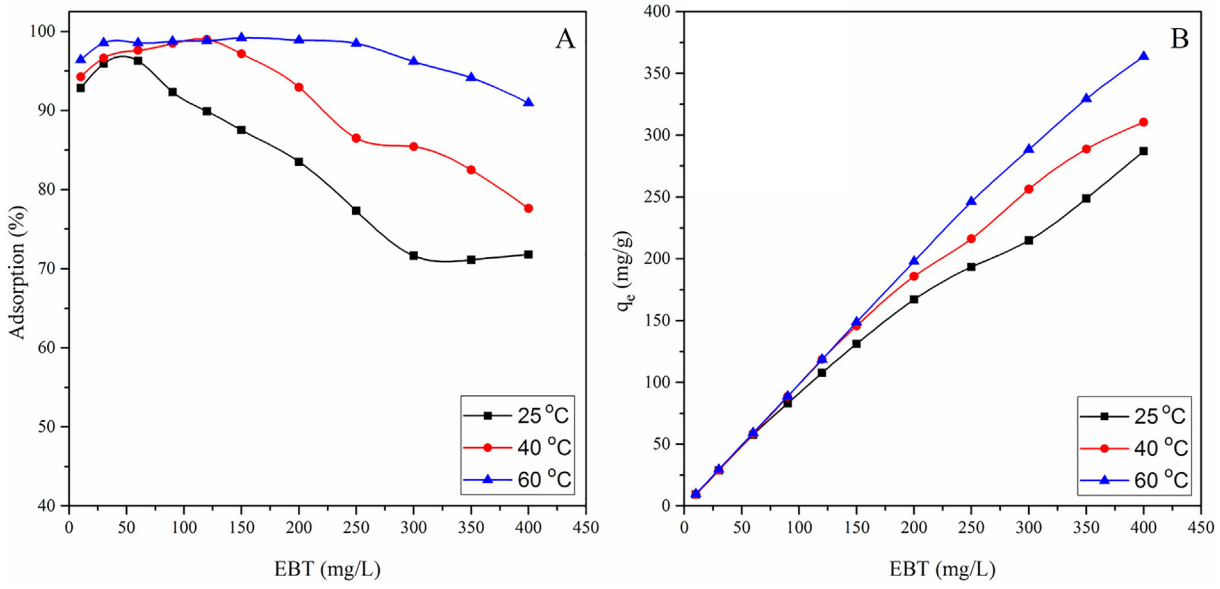

Fig. 3. Effect of temperature and initial concentration of EBT on the percent adsorption (A) and adsorption per unit mass (B), at pH = 2.0, m/V = 1.0 g/L, and t = 24 h.

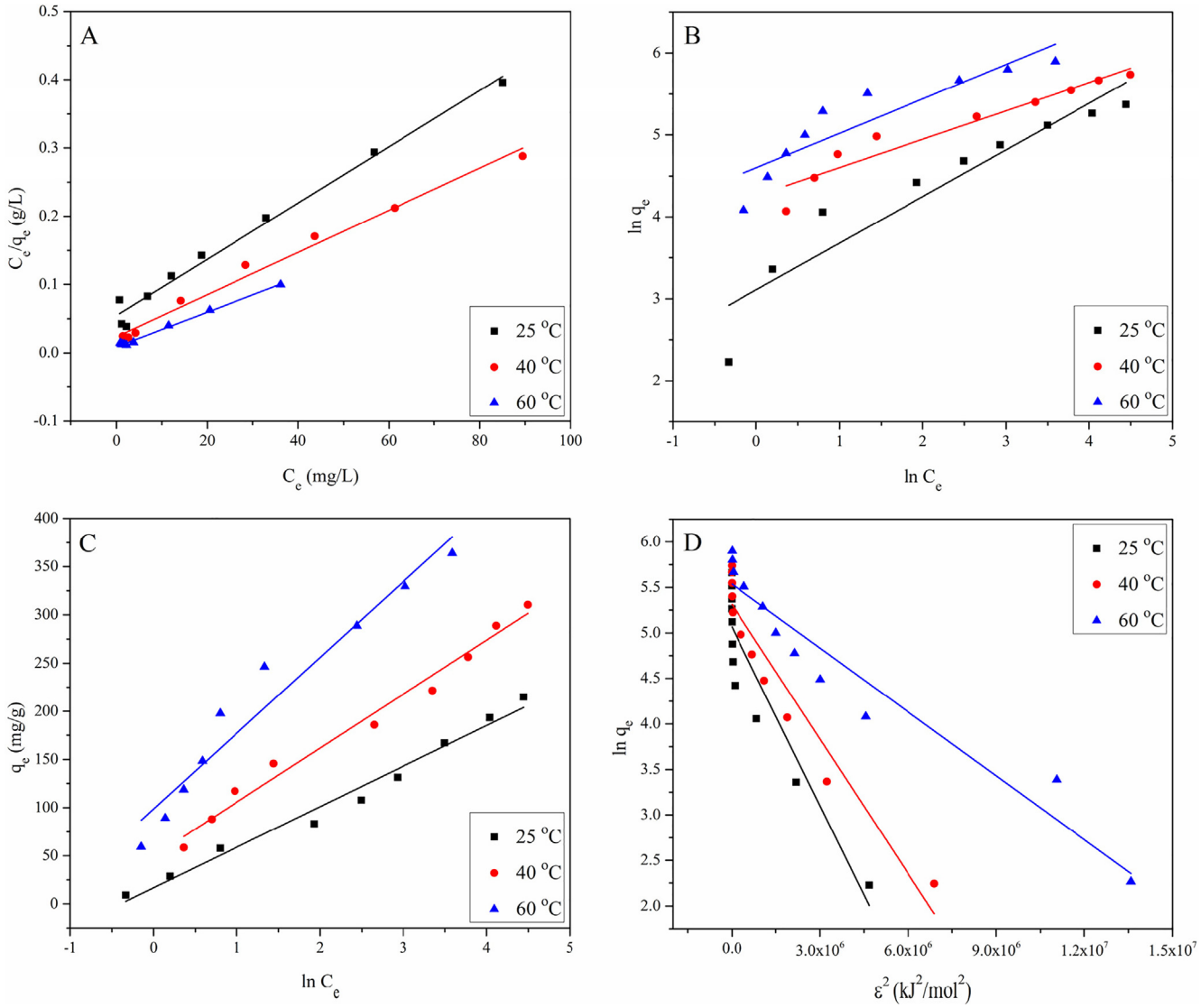

Fig. 4. Isotherm plots, Langmuir (A), Freundlich (B), Temkin (C) and Dubinin-Radushkevich model (D) for EBT adsorption onto MASTL, at pH = 2.0, m/V = 1.0 g/L, and t = 24 h.

the Langmuir isotherm plot of EBT adsorption onto MASTL. The respective values of q_m, b and R^2 are listed in Table 1. It shows that the equilibrium data were in good agreement with Langmuir adsorption isotherm model.

The dimensionless constant separation factor R_L, given in Eq. (5), expresses the most important characteristics of the Langmuir isotherm [30]:

$$R_L = \frac{1}{1 + bC_o} \tag{5}$$

The values of R_L describe the nature of equilibrium and falls to zero for the irreversible process (i.e., $R_L = 0$). The equilibrium is more favourable when $0 < R_L < 1$ and linear when $R_L = 1$, whereas the equilibrium is unfavourable when $R_L > 1$ [31]. The R_L values obtained for EBT adsorption were plotted as a function of EBT initial concentrations and shown in Fig. 5. It shows that the R_L values vary with initial concentration as well as with temperature and ranged from 0.0319 to 0.5693 at 25 °C, from 0.0185 to 0.4301 at 40 °C and from 0.0085 to 0.2551 at 60 °C. From these values it was concluded that at all temperatures, the adsorption of EBT was more favourable at low concentrations and became nearly irreversible at high initial concentrations.

The Freundlich isotherm, an empirical equation, is one of the oldest nonlinear isotherms that describes the heterogeneous adsorption of solutes from liquid to solid surfaces, was also applied to check its applicability towards the adsorption of EBT onto MASTL. The Freundlich isotherm can be expressed as [32]:

$$lnq_e = lnK_F + \frac{1}{n}(lnC_e) \tag{6}$$

where K_F (mg^{1-n}·L^n/g) indicates the approximate adsorption capacity, whereas $1/n$ represents the heterogeneity of the system. The smaller the value of $1/n$ is, the greater the expected heterogeneity of the system [33]. The parameters K_F and n are the characteristics of the sorbent-sorbate system and can be determined respectively from the intercept and slope of the linear plot of lnq_e vs. lnC_e. Different values of n represent different adsorption behaviours. Based on the previous studies, Voudrias et al. [34] mentioned that $n = 1$ showed that the partition between the two phases was independent of the pollutant concentration, $n > 1$ represented a normal adsorption process, whereas $n < 1$ indicated cooperative adsorption process. Similarly, the n value between 1 and 10 represented a favourable adsorption process. lnq_e was plotted against lnC_e (Fig. 4B) to evaluate the adsorption data on Freundlich isotherm

Table 1
Langmuir, Freundlich, Temkin and Dubinin-Radushkevich model constants and correlation coefficients for the adsorption of EBT onto MASTL.

Langmuir isotherm				
Temperature (°C)	q_m (mg/g)	b (L/mg)		R^2
25	242.72	0.0756		0.9859
40	323.63	0.1325		0.9889
60	393.70	0.2919		0.9946
Temkin isotherm				
Temperature (K)	A (L/g)	B (J/mol)		R^2
25	1.49	42.10		0.9814
40	2.43	56.027		0.9828
60	3.51	78.6126		0.9499
Freundlich isotherm				
Temperature (K)	n	1/n	K_F ($mg^{1-n}.L^n/g$)	R^2
25	1.7562	0.5694	22.41	0.8918
40	2.8873	0.3463	70.48	0.9285
60	2.3793	0.4203	99.47	0.8224
Dubinin-Radushkevich				
Temperature (K)	q_m (mg/g)	$K_E \times 10^{-7}$ (mol^2/kJ^2)	E (kJ/mol)	R^2
25	158.52	6.55	0.8737	0.8608
40	203.42	4.93	1.0071	0.9271
60	253.74	2.34	1.4618	0.9373

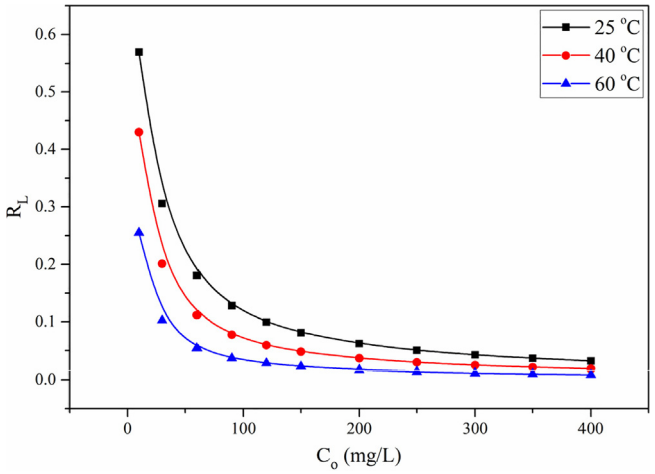

Fig. 5. The separation factors for EBT adsorption onto MASTL at different temperatures.

and its ability to describe the adsorption of EBT onto MASTL at three different temperatures (i.e., 25, 40 and 60 °C). The relative values of K_F, n and linear regression (R^2) are tabulated in Table 1, which showed that the values of n were between 1 and 10, indicating that the adsorption of EBT onto MASTL was favourable. However, the lower R^2 values indicated that the data were not in close proximity with Freundlich isotherm and fit well with the Langmuir isotherm model. This also indicated that the adsorbent surface was homogeneous and the adsorption process resulted in the monolayer coverage of the adsorbent surface [35].

Temkin model is a proper isotherm model for the multi-layer chemical adsorption based on strong electrostatic interactions between positive and negative charges [36]. Temkin equation can be expressed as:

$$q_e = \frac{RT}{b}\ln(AC_e) \tag{7}$$

Eq. (7) can be transformed into linear form as:

$$q_e = \frac{RT}{b_T}lnA + \frac{RT}{b}lnC_e \tag{8}$$

$$q_e = BlnA + \frac{RT}{b}lnC_e \tag{9}$$

where:

- B = constant related to the heat of adsorption (J/mol)
- A = equilibrium binding constant (L/g), corresponding to the maximum binding energy
- R = universal gas constant (8.314 J/mol·K)
- T = absolute temperature (K)
- b = adsorption constant (J/mol·K)

Fig. 4C shows the Temkin model for the adsorption of EBT onto MASTL and the calculated isotherm constants are listed in Table 1.

In order to calculate the mean free energy (E), to determine the nature of sorption reaction, Dubinin-Radushkevich (D-R) isotherm [37] was applied to evaluate the adsorption of EBT onto MASTL. It was basically formulated to describe the adsorption processes occurring on both homogeneous and heterogeneous surfaces that followed the pore filling mechanism. The D-R equation can be expressed as [38]:

$$q_e = q_m.exp(-K_E\varepsilon^2) \tag{10}$$

Eq. (10) can be converted into linear form by taking natural log of both sides:

$$lnq_e = lnq_m - K_E\varepsilon^2 \tag{11}$$

where K_E (mol^2/kJ^2) is the adsorption energy constant and is related to the mean free energy (E, J/mol·K) of sorption through the following equation [39]:

$$E = \frac{1}{\sqrt{2K_E}} \tag{12}$$

Similarly, ε (kJ/mol) is a constant called the Polanyi potential and can be calculated from Eq. (13):

$$\varepsilon = RT\ln\left(1 + \frac{1}{C_e}\right) \tag{13}$$

Here it should be clear that Dubinin-Radushkevich isotherm model cannot be simplified like Langmuir and Freundlich isotherm models. However, it is a straight line equation and the plot of $\ln q_e$ vs. ε^2 should give a straight line with intercept equal to $\ln q_m$ and slope equal to K_E as shown in Fig. 4D. The values of the parameters obtained from Dubinin-Radushkevich isotherm model are listed in Table 1. Results showed that the amount of theoretical monolayer sorption capacity (q_m) increased with the increase in temperature,

Table 2
Comparison of equilibrium monolayer adsorption capacity of EBT on different adsorbents.

Adsorbent	q_m (mg/g)	Ref.
Calcined MgAl-LDH	540.91	[42]
Calcined CoAl-LDH	419.87	
Calcined NiFe-LDH	132.49	
Maize stem tissue	167.01	[19]
Activated carbon from waste rice hulls	160.36	[16]
MgAl-LDH	128.20	[17]
Magnetite/pectin NPs	103.41	[15]
Magnetite/silica/pectin NPs	80.15	
Eucalyptus bark	52.37	[13]
$NiFe_2O_4$ nanoparticles	47.00	[18]
Microwave treated almond shell	29.41	[43]
Cold plasma treated almond shell	18.18	
Untreated almond shell	6.06	
Hydrophobic cross-linked polyzwitterionic acid	15.90	[44]
MASTL	242.72	This work

which may be due to either the increase in the number of active adsorption sites or an increase in the diffusion of ions or molecules of EBT.

The mean free energy of sorption, which is the amount of energy released when one mole of ions is transferred to the solid surface from infinity in solution, was calculated from Eq. (12). The magnitude of mean free energy of adsorption describes the nature of sorption reaction. The E value in the range of 1–8 kJ/mol indicates physisorption, 8–16 kJ/mol indicates an ion-exchange mechanism [40] and 16–40 kJ/mol indicates a chemisorption mechanism [41]. The data in Table 1 showed that the values of E were lower than 8 kJ/mol, which indicated a physisorption mechanism. Data in Table 1 also showed the correlation coefficients (R^2) were in the order: Langmuir > Temkin > Freundlich. The monolayer maximum adsorption capacity (q_m = 242.72 mg/g at 25 °C) of EBT onto MASTL was compared with other adsorbents in Table 2. It indicated that except Calcined MgAl-LDH and Calcined CoAl-LDH [42], the adsorption capacity of MASTL was higher than other materials. In addition to high adsorption capacity, low-cost, environmentally safe, simple and easy preparation recommends MASTL as a suitable material for the removal of EBT from aqueous solutions.

3.8. Adsorption kinetics

Kinetic models have been used to investigate the mechanism of sorption reaction and the potential rate controlling steps such as mass transport and the way the chemical reaction occurs. The commonly used kinetic models, the Lagergren pseudo-first-order and Ho's pseudo-second-order models were used to investigate the kinetics of EBT adsorption onto MASTL.

The pseudo-first-order kinetic model assumes that the adsorption rate is proportional to the population of the free adsorption sites (q_e-q_t) available on the adsorbent's surface rather than the adsorbate concentration in solution. The pseudo-first-order kinetic equation can be described as [45]:

$$\frac{dq_t}{dt} = k_1(q_e - q_t) \tag{14}$$

where k_1 (1/min) is the equilibrium constant for pseudo-first-order kinetic model. Changing the time from t = 0 to t = t, the adsorption changes from q_t = 0 to q_t = q_t, such that:

$$\int_{t=0}^{t=t} \frac{dq_t}{dt} = k_1 \int_{q_t=0}^{q_t=t} (q_e - q_t) \tag{15}$$

$$\ln\left(\frac{q_e}{q_e - q_t}\right) = kt \tag{16}$$

$$q_t = q_e(1 - e^{-kt}) \tag{17}$$

Taking log of both sides, Eq. (17) can be rearranged to the following linear form:

$$\log(q_e - q_t) = \log q_e - \frac{k_1}{2.303}t \tag{18}$$

The first-order rate constant (k_1) and equilibrium concentration (q_e) determined from the equation of first-order model are presented in Table 3. Fig. 6A shows that the pseudo-first-order model gives a straight line with good fitness and high R^2 values at both 25 and 40 °C. However, it can be seen from Table 3 that the values of $q_{e,cal}$ are not relevant to the values of $q_{e,\exp}$, which showed that good fitness is not necessarily the one with high correlation coefficient.

The pseudo-second-order kinetic model is based on the sorption capacity of the adsorbent in which the chemical reaction seems significant in the rate-controlling step, and follows chemisorption mechanism. The Ho's pseudo-second-order kinetic model can be expressed as [46]:

$$\frac{dq_t}{dt} = k_2(q_e - q_t)^2 \tag{19}$$

Integrating and applying the boundary conditions (t = 0 to t = t and q_t = 0 to q_t = q_t), Eq. (19) can be rearranged as:

$$\frac{1}{q_e - q_t} = \frac{1}{q_e} + k_2 t \tag{20}$$

The nonlinear Eq. (20) can be rearranged to the following linearized form:

$$\frac{t}{q_t} = \frac{1}{k_2 q_e^2} + \frac{1}{q_e}t \tag{21}$$

where q_e (mg/g) is the equilibrium adsorption capacity and k_2 is the second-order rate constant (g/mg·min), and were calculated respectively from the slope and intercept of the plot t/q_t vs. t (Fig. 6B). The experimental values of $q_{e,\exp}$ and the calculated values of k_2 and $q_{e,cal}$, obtained from pseudo-second-order model are tabulated in Table 3. It shows that pseudo-second-order kinetic model best explains the EBT adsorption data, suggesting that the adsorption is chemical in nature. A similar result was reported for EBT adsorp-

Table 3
Kinetic parameters for EBT adsorption onto MASTL. $q_{e,\exp}$ = 57.70 and 57.99 mg/g at 25 and 40 °C respectively.

Model	Parameters		
		25 °C	40 °C
Pseudo-first-order	k_1 (1/min)	0.0196	0.0368
	$q_{e,cal}$ (mg/g)	39.10	42.24
	R^2	0.9965	0.9980
Pseudo-second-order	k_2 (g/mg·min)	0.0009	0.0162
	$q_{e,cal}$ (mg/g)	62.11	61.58
	h (mg/g·min)	3.34	6.22
	$t_{1/2}$ (min)	18.59	9.91
	R^2	0.9977	0.9995
Intraparticle diffusion	k_{p1}	3.8443	3.9502
	(mg/g·min$^{1/2}$)	14.77	19.90
Stage-I	C_1 (mg/g)	0.9990	0.9611
	R_1^2		
Stage-II	k_{p2}	0.8460	0.1232
	(mg/g·min$^{1/2}$)	44.74	56.26
	C_2 (mg/g)	0.9638	0.7452
	R_2^2		
Stage-III	k_{p3}	0.1919	–
	(mg/g·min$^{1/2}$)	54.62	–
	C_3 (mg/g)	0.9250	–
	R_3^2		

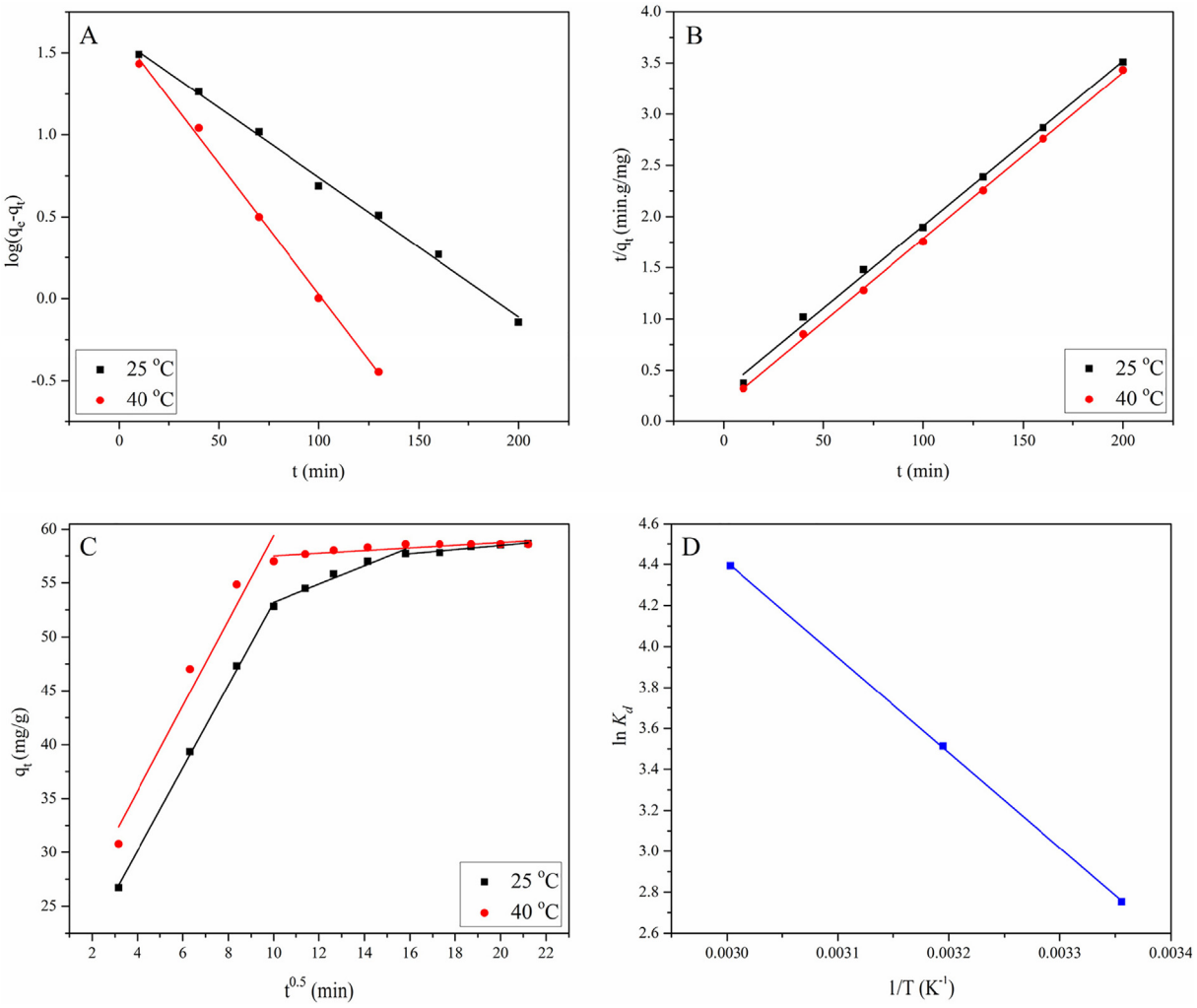

Fig. 6. The fitting of pseudo-first-order (A), pseudo-second-order (B), Intraparticle diffusion model (C) and Van't Hoff plot (D), for EBT adsorption onto MASTL, at pH = 2.0, m/V = 1.0 g/L, $C[EBT]_{initial}$ = 60 mg/L.

tion from aqueous solution using activated carbon [16]. As the data follow both the pseudo-first and second-order kinetics, we concluded that the adsorption of EBT is physicochemical in nature, which was very similar to the previously reported results [47].

The second-order rate constant k_2, can be used to determine the initial adsorption rate, h (mg/g·min) [48], when q_t/t reaches to zero then:

$$h = k_2 q_e^2 \tag{22}$$

Similarly, the half-equilibrium time, $t_{1/2}$ (min) for EBT adsorption onto MASTL was determined from Eq. (23) and the results obtained are listed in Table 3.

$$t_{1/2} = \frac{1}{k_2 q_e} \tag{23}$$

It shows that by increasing the temperature from 25 to 40 °C, the initial adsorption rate increased from 3.34 to 6.22 mg/g·min, whereas the half-equilibrium time decreased by half i.e., from 18.59 to 9.91 min. From these results we concluded that the adsorption of EBT onto MASTL was endothermic in nature [49].

Furthermore, the activation energy was calculated from the Arrhenius equation [50] as:

$$lnk = lnA - \frac{E_a}{RT} \tag{24}$$

where k is the kinetic rate constant, A is the pre-exponential factor (1/min) and E_a is the energy of activation (kJ/mol).

For convenience Eq. (24) was transformed into two points form as:

$$E_a = \frac{RT_1T_2}{T_1 - T_2} ln\left(\frac{k_1}{k_2}\right) \tag{25}$$

where k_1 and k_2 are the first-order rate constants obtained at T_1 and T_2 respectively. The activation energy calculated from Eq. (25) was found to be 32.70 kJ/mol, which is lower than the energy of chemisorption (40 kJ/mol). These results indicated that Van der Waals forces were also involved in the adsorption process [51].

3.9. Intraparticle diffusion

The above kinetic models were not able to explain the diffusion mechanism. Therefore, the intraparticle diffusion model based on Weber and Morris theory [52] was applied. It is an empirical relationship, applicable to most of the adsorption processes, where the uptake varies almost proportionally with $t^{0.5}$ rather than the contact time (t). According to this theory:

$$q_t = k_{pi} t^{0.5} + C_i \tag{26}$$

where k_{pi} (mg/g·min$^{1/2}$) is the rate parameter of the stage i and can be obtained from the slope of the plot q_t vs. $t^{0.5}$. The values of k_{pi}, C_i

and R^2 obtained from the model are listed in Table 3. The intercept C_i, of the stage i, is proportional to the thickness of the boundary layer. Fig. 6C shows that the intraparticle diffusion diagram has three regions at 25 °C and two regions at 40 °C. The high adsorption rate in the first region (both at 25 and 40 °C) can be attributed to the high initial concentration of EBT and free adsorption sites on MASTL surfaces. However, the adsorption rate moderated in the second region, where the intraparticle diffusion is the rate limiting step. In the third region, the adsorption is not very significant and the intraparticle diffusion became very slow due to the extremely low EBT concentration left in the solution. Moreover, it is obvious from Fig. 6C, that the plots are not linear over the whole range of contact time, implying that the intraparticle diffusion was not the only mechanism of adsorption.

3.10. Thermodynamic parameters

Variations of EBT adsorption data with temperature were used to calculate the thermodynamic parameters, i.e., change in Gibbs free energy (ΔG^o), enthalpy change (ΔH^o) and entropy change (ΔS^o), according to the following equation:

$$\Delta G^o = -RTlnK_d \quad (27)$$

where K_d is the sorption distribution coefficient and R (8.314 J/mol·K) is the ideal gas constant. Values of K_d were calculated from the intercept of the plot $\ln(q_e/C_e)$ vs. C_e [53].

Gibbs free energy of adsorption was calculated from Eq. (28):

$$\Delta G^o = \Delta H^o - T\Delta S^o \quad (28)$$

Putting for ΔG^o, Eq. (28) can be rearranged as:

$$lnK_d = \frac{\Delta S^o}{R} - \frac{\Delta H^o}{R}\cdot\frac{1}{T} \quad (29)$$

The values of ΔS^o and ΔH^o were calculated from the intercept and slope of the plot $\ln K_d$ vs. $1/T$ (Fig. 6D), and are listed in Table 4.

The positive value of ΔH^o indicated that the adsorption of EBT over the surface of MASTL was endothermic. The value of ΔH^o (31.82 kJ/mol) was far lower than the heat of chemisorption, which is in the range of 80–200 kJ/mol [54]. One possible interpretation to the positive ΔH^o values was that the EBT was well solvated in aqueous solution. In order to adsorb on the surface of MASTL, the EBT molecules should be denuded of the hydration sheath, which needs energy. However, the dehydration energy exceeded the energy released when EBT ions or molecules are attaching to the MASTL surface. In other words, the dehydration of the ions was an endothermic process and the endothermicity of the desolvation process extensively exceeded that of the enthalpy of adsorption [55]. The positive ΔS^o value (189.32 J/mol·K) indicated that the adsorption was random at solid-solution interface and reflected the affinity of MASTL towards EBT, which also showed some structural changes in the adsorbent during the adsorption process [56]. The negative ΔG^o values (−24.55, −27.55 and −31.18 kJ/mol at 298, 313 and 333 K respectively) indicated that the adsorption was fairly feasible and spontaneous under the applied conditions. The decrease in ΔG^o values with the increase of temperature suggested that the sorption of EBT was a favourable process, because of its rapid dehydration at higher temperature. ΔG^o values from 0 to −20 kJ/mol indicates physisorption, while more negative than −40 kJ/mol represents chemisorption. Similarly, adsorption is controlled by both physical and chemical interactions, when the corresponding values of ΔG^o fall in the range of −20 to −40 kJ/mol [57]. The data in Table 4 showed that ΔG^o values were in the range of −20 to −40 kJ/mol, suggesting that the adsorption process was physicochemical in nature. Positive values of ΔS^o indicated that the adsorption process was fairly random at solid/solution interface. The thermodynamic study concluded that the adsorption of EBT onto STL was thermally feasible, spontaneous, endothermic, highly random at solid/solution interface and physicochemical in nature. However, like the adsorption of astrazon red 6B onto STL [23], the physical adsorption was dominant over the chemical.

3.11. Adsorption mechanism

FT-IR technique was applied to study the active sites of the adsorbents and to determine their interactions with the dye molecules, which was helpful to understand the interaction mechanism [58]. The FT-IR spectrum (Fig. 1C) showed that MASTL had a number of functional groups, such as –OH, -C=O and $-SO_3$. These groups have different forms under different pH conditions. EBT is a diprotic anionic dye due to its sulphonate groups ($-SO_3$) and exists as negatively charged in aqueous solutions. Fig. 7B shows that the adsorption of EBT was strongly pH dependent and the highest adsorption was found at pH 2.0. At $pH < pH_{pzc}$ (4.6), the surface of MASTL was positive, whereas that of EBT was negative according to the following reactions:

$$MASTL - OH + H^+ \leftrightarrow MASTL - OH_2^+$$

$$EBT - SO_3^-Na^+ \leftrightarrow EBT - SO_3^- + Na^+$$

As a result, the sorption process was promoted through electrostatic attractions between the two counter ions [59] as:

$$MASTL - OH_2^+ + EBT - SO_3^- \leftrightarrow MASTL - OH_2^+ \ldots SO_3^-EBT$$

The electrostatic attractions suggested chemisorption of EBT onto MASTL. It is clear from Fig. 7B that a continuous decrease in the dye adsorption was found with the increase of pH. Because, by doing so, the positive surface charge density of MASTL decreased, which resulted in weakening of its attractive forces towards anionic EBT. At $pH > pH_{pzc}$, the MASTL surface became negatively charged, which resulted in high electrostatic repulsion and lead to a very low adsorption. Moreover, FT-IR technique provided informations of the interactions of the active sites of the adsorbents with different functional groups of the dye. One can see from the FT-IR spectrum of MASTL after EBT adsorption (Fig. 1D), that the peak at 3402 cm^{-1} shifted to lower wavelength of 3377 cm^{-1}, which indicated that the hydrogen bonding (formed by the –OH of MASTL and N or O of EBT) might involve in the adsorption process [60]. Though, no considerable changes were observed in the positions of peaks from 1700 cm^{-1} to 1000 cm^{-1}, all the peaks underwent a tremendous decrease in the absorption intensity, which indicated the successful attachment of the dye with the adsorbent.

Table 4
Thermodynamic constants for EBT adsorption onto MASTL.

1/T (1/K)	$\ln K_d$	T (K)	ΔG^o (kJ/mol)	ΔH^o (kJ/mol)	ΔS^o (J/mol·K)
0.0034	9.91	298	−24.55	31.82	189.32
0.0032	10.58	313	−27.55		
0.0030	11.26	333	−31.18		

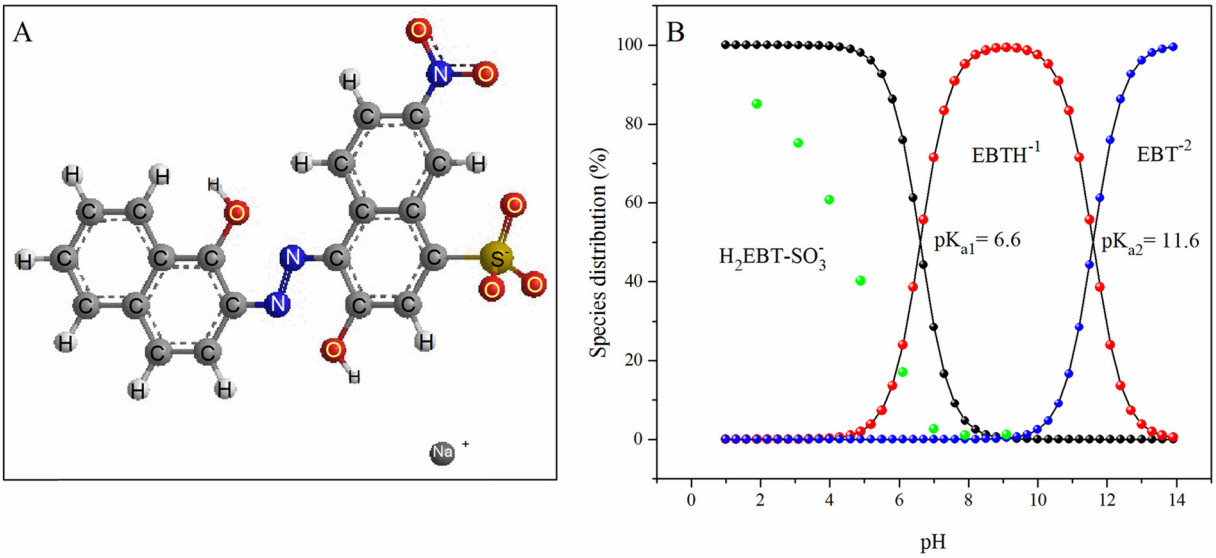

Fig. 7. Molecular structure of EBT (A) and distribution of various species of EBT and its percent adsorption (green balls) as a function of pH (B).

4. Conclusion

The results demonstrated that the spent tea leaves, an abundantly available solid waste, can be used for the efficient removal of EBT from aqueous solutions. The microwave treatment tremendously increased the surface area of the STL. Excellent recoveries of EBT were obtained with small amount of MASTL. Due to the protonation-deprotonation reaction, the MASTL surface was positive at pH < pH_{pzc}, neutral at pH = pH_{pzc} and negative at pH > pH_{pzc}. The adsorption of EBT was strongly dependent on the pH of the medium. The removal percentage of EBT increased with the increase of the solid content however, it had inverse effect on q_e values. Temperature had a positive effect on the adsorption rate and the equilibrium time decreased from 250 min to 160 min by increasing temperature from 25 to 40 °C. Adsorption data were well simulated by Langmuir isotherm model with maximum monolayer adsorption capacity of 242.72 mg/g at 25 °C. Similarly, kinetic data were in good agreement with both pseudo-first and second-order kinetic models. Thermodynamically, the adsorption of EBT onto MASTL was feasible, spontaneous, endothermic and random at solid-solution interface. Due to abundant availability and strong physicochemical interactions with EBT, MASTL can be used as cost-effective green adsorbent for the removal of EBT from wastewaters.

Acknowledgements

Financial support from Chinese government under China Scholarship Council (CSC) for foreign postgraduate students, NSFC (21577032) and the Fundamental Research Funds for the Central Universities (JB2015001) are acknowledged.

References

[1] Monvisade P, Siriphannon P. Chitosan intercalated montmorillonite: preparation, characterization and cationic dye adsorption. Appl Clay Sci 2009;42:427–31. doi: https://doi.org/10.1016/j.clay.2008.04.013.
[2] Barka N, Abdennouri M, Makhfouk MEL. Removal of Methylene Blue and Eriochrome Black T from aqueous solutions by biosorption on Scolymus hispanicus L.: kinetics, equilibrium and thermodynamics. J Taiwan Inst Chem Eng 2011;42:320–6. doi: https://doi.org/10.1016/j.jtice.2010.07.004.
[3] Mohammadi N, Khani H, Gupta VK, Amereh E, Agarwal S. Adsorption process of methyl orange dye onto mesoporous carbon material-kinetic and thermodynamic studies. J Colloid Interface Sci 2011;362:457–62. doi: https://doi.org/10.1016/j.jcis.2011.06.067.
[4] Lin S-H, Juang R-S, Wang Y-H. Adsorption of acid dye from water onto pristine and acid-activated clays in fixed beds. J Hazard Mater 2004;113:195–200. doi: https://doi.org/10.1016/j.jhazmat.2004.06.028.
[5] Ejhieh AN, Khorsandi M. Photodecolorization of Eriochrome Black T using NiS–P zeolite as a heterogeneous catalyst. J Hazard Mater 2010;176:629–37. doi: https://doi.org/10.1016/j.jhazmat.2009.11.077.
[6] Ahmad A, Hameed B. Fixed-bed adsorption of reactive azo dye onto granular activated carbon prepared from waste. J Hazard Mater 2010;175:298–303. doi: https://doi.org/10.1016/j.jhazmat.2009.10.003.
[7] Gerçel Ö, Gerçel HF, Koparal AS, Öğütveren ÜB. Removal of disperse dye from aqueous solution by novel adsorbent prepared from biomass plant material. J Hazard Mater 2008;160:668–74. doi: https://doi.org/10.1016/j.jhazmat.2008.03.039.
[8] Sun J, Qiao L, Sun S, Wang G. Photocatalytic degradation of Orange G on nitrogen-doped TiO_2 catalysts under visible light and sunlight irradiation. J Hazard Mater 2008;155:312–9. doi: https://doi.org/10.1016/j.jhazmat.2007.11.062.
[9] García-Montaño J, Ruiz N, Munoz I, et al. Environmental assessment of different photo-Fenton approaches for commercial reactive dye removal. J Hazard Mater 2006;138:218–25. doi: https://doi.org/10.1016/j.jhazmat.2006.05.061.
[10] Azmi W, Sani RK, Banerjee UC. Biodegradation of triphenylmethane dyes. Enzyme Microb Technol 1998;22:185–91. doi: https://doi.org/10.1016/S0141-0229(97)00159-2.
[11] Crini G. Non-conventional low-cost adsorbents for dye removal: a review. Bioresour Technol 2006;97:1061–85. doi: https://doi.org/10.1016/j.biortech.2005.05.001.
[12] Robinson T, Chandran B, Nigam P. Removal of dyes from a synthetic textile dye effluent by biosorption on apple pomace and wheat straw. Water Res 2002;36:2824–30. doi: https://doi.org/10.1016/S0043-1354(01)00521-8.
[13] Dave PN, Kaur S, Khosla E. Removal of Eriochrom black-T by adsorption on to eucalyptus bark using green technology Indian J Chem Technol 2011;18:53–60.
[14] Hameed B, Din AM, Ahmad A. Adsorption of methylene blue onto bamboo-based activated carbon: kinetics and equilibrium studies. J Hazard Mater 2007;141:819–25. doi: https://doi.org/10.1016/j.jhazmat.2006.07.049.
[15] Attallah O, Al-Ghobashy M, Nebsen M, Salem M. Removal of cationic and anionic dyes from aqueous solution with magnetite/pectin and magnetite/silica/pectin hybrid nanocomposites: kinetic, isotherm and mechanism analysis. RSC Adv 2016;6:11461–80. doi: https://doi.org/10.1039/c5ra23452b.
[16] de Luna MDG, Flores ED, Genuino DAD, Futalan CM, Wan M-W. Adsorption of Eriochrome Black T (EBT) dye using activated carbon prepared from waste rice hulls-Optimization, isotherm and kinetic studies. J Taiwan Inst Chem Eng 2013;44:646–53. doi: https://doi.org/10.1016/j.jtice.2013.01.010.
[17] Yasin Y, Abdul Malek AH, Sumari SM. Adsorption of eriochrome black dye from aqueous solution onto anionic layered double hydroxides. Orient J Chem 2010;26:1293–8.
[18] Moeinpour F, Alimoradi A, Kazemi M. Efficient removal of Eriochrome black-T from aqueous solution using NiFe2O4 magnetic nanoparticles. J Environ Health Sci Eng 2014;12:1–7. doi: https://doi.org/10.1186/s40201-014-0112-8.
[19] Vučurović VM, Razmovski RN, Miljić UD, Puškaš VS. Removal of cationic and anionic azo dyes from aqueous solutions by adsorption on maize stem tissue. J Taiwan Inst Chem Eng 2014;45:1700–8. doi: https://doi.org/10.1016/j.jtice.2013.12.020.
[20] Mokgalaka N, McCrindle R, Botha B. Multielement analysis of tea leaves by inductively coupled plasma optical emission spectrometry using slurry

nebulisation. J Anal At Spectrom 2004;19:1375–8. doi: https://doi.org/10.1039/B407416E.
[21] Panneerselvam P, Morad N, Tan KA. Magnetic nanoparticle (Fe_3O_4) impregnated onto tea waste for the removal of nickel(II) from aqueous solution. J Hazard Mater 2011;186:160–8. doi: https://doi.org/10.1016/j.jhazmat.2010.10.102.
[22] Hameed BH. Spent tea leaves: A new non-conventional and low-cost adsorbent for removal of basic dye from aqueous solutions. J Hazard Mater 2009;161:753–9. doi: https://doi.org/10.1016/j.jhazmat.2008.04.019.
[23] Özbaş EE, Öngen A, Gökçe CE. Removal of astrazon red 6B from aqueous solution using waste tea and spent tea bag. Desalin Water Treat 2013;51:7523–35. doi: https://doi.org/10.1080/19443994.2013.792161.
[24] Khosla E, Kaur S, Dave PN. Tea waste as adsorbent for ionic dyes. Desalin Water Treat 2013;51:6552–61. doi: https://doi.org/10.1080/19443994.2013.791776.
[25] Bagheri H, Afkhami A, Saber-Tehrani M, Khoshsafar H. Preparation and characterization of magnetic nanocomposite of Schiff base/silica/magnetite as a preconcentration phase for the trace determination of heavy metal ions in water, food and biological samples using atomic absorption spectrometry. Talanta 2012;97:87–95. doi: https://doi.org/10.1016/j.talanta.2012.03.066.
[26] Eroğlu H, Yapici S, Nuhoğlu Ç, Varoğlu E. An environmentally friendly process; Adsorption of radionuclide Tl-201 on fibrous waste tea. J Hazard Mater 2009;163:607–17. doi: https://doi.org/10.1016/j.jhazmat.2008.07.076.
[27] Malkoc E, Nuhoglu Y. Removal of Ni(II) ions from aqueous solutions using waste of tea factory: adsorption on a fixed-bed column. J Hazard Mater 2006;135:328–36. doi: https://doi.org/10.1016/j.jhazmat.2005.11.070.
[28] Wan S, Ma Z, Xue Y, et al. Sorption of lead (II), cadmium (II), and copper (II) ions from aqueous solutions using tea waste. Ind Eng Chem Res 2014;53:3629–35. doi: https://doi.org/10.1021/ie402510s.
[29] Karatapanis AE, Fiamegos Y, Stalikas CD. Silica-modified magnetic nanoparticles functionalized with cetylpyridinium bromide for the preconcentration of metals after complexation with 8-hydroxyquinoline. Talanta 2011;84:834–9. doi: https://doi.org/10.1016/j.talanta.2011.02.013.
[30] Weber T, Chakravorti R. Pore and solid diffusion models for fixed-bed adsorbers AIChE Journal 1974;20:228–38. doi: https://doi.org/10.1002/aic.690200204.
[31] Hall KR, Eagleton LC, Acrivos A, Vermeulen T. Pore-and solid-diffusion kinetics in fixed-bed adsorption under constant-pattern conditions. I&EC Fundam 1966;5:212–23. doi: https://doi.org/10.1021/i160018a011.
[32] Romero-González J, Peralta-Videa JR, Rodríguez E, Ramirez SL, Gardea-Torresdey JL, Ramirez SL. Determination of thermodynamic parameters of Cr (VI) adsorption from aqueous solution onto Agave lechuguilla biomass. J Chem Thermodyn 2005;37:343–7. doi: https://doi.org/10.1016/j.jct.2004.09.013.
[33] Goldberg S, Tabatabai M, Al-Amoodi L, Dick W. Equations and models describing adsorption processes in soils. Soil Sci. Soc. Am. Book Ser. 2005;8:489–517.
[34] Voudrias E, Fytianos K, Bozani E. Sorption-desorption isotherms of dyes from aqueous solutions and wastewaters with different sorbent materials. Global NEST 2002;4:75–83.
[35] Mohan SV, Karthikeyan J. Removal of lignin and tannin color from aqueous solution by adsorption on to activated carbon solution by adsorption on to activated charcoal. Environ Pollut 1997;97:183–7. doi: https://doi.org/10.1016/S0269-7491(97)00025-0.
[36] Ma Q, Song T-Y, Yuan P, Wang C, Su X-G. QDs-labeled microspheres for the adsorption of rabbit immunoglobulin G and fluoroimmunoassay. Colloids Surf, B 2008;64:248–54. doi: https://doi.org/10.1016/j.colsurfb.2008.01.027.
[37] Dubinin M, Radushkevich L. Equation of the characteristic curve of activated charcoal. Chem. Zentr 1947;1:875.
[38] Chen X. Modeling of Experimental Adsorption Isotherm Data. Information 2015;6:14–22. doi: https://doi.org/10.3390/info6010014.
[39] Hobson JP. Physical adsorption isotherms extending from ultrahigh vacuum to vapor pressure. J Phys Chem 1969;73:2720–7. doi: https://doi.org/10.1021/j100842a045.
[40] Mahramanlioglu M, Kizilcikli I, Bicer IO. Adsorption of fluoride from aqueous solution by acid treated spent bleaching earth. J Fluorine Chem 2002;115:41–7. doi: https://doi.org/10.1016/s0022-1139(02)00003-9.
[41] Fan S, Tang J, Wang Y, et al. Biochar prepared from co-pyrolysis of municipal sewage sludge and tea waste for the adsorption of methylene blue from aqueous solutions: kinetics, isotherm, thermodynamic and mechanism. J Mol Liq 2016;220:432–41. doi: https://doi.org/10.1016/j.molliq.2016.04.107.
[42] Zubair M, Jarrah N, Manzar MS, et al. Adsorption of eriochrome black T from aqueous phase on MgAl-, CoAl-and NiFe-calcined layered double hydroxides: Kinetic, equilibrium and thermodynamic studies. J Mol Liq 2017;230:344–52. doi: https://doi.org/10.1016/j.molliq.2017.01.031.
[43] Şahin Ö, Saka C, Kutluay S. Cold plasma and microwave radiation applications on almond shell surface and its effects on the adsorption of Eriochrome Black T. J Ind Eng Chem 2013;19:1617–23. doi: https://doi.org/10.1016/j.jiec.2013.01.032.
[44] Saleh TA, Muhammad AM, Ali SA. Synthesis of hydrophobic cross-linked polyzwitterionic acid for simultaneous sorption of Eriochrome black T and chromium ions from binary hazardous waters. J Colloid Interface Sci 2016;468:324–33. doi: https://doi.org/10.1016/j.jcis.2016.01.057.
[45] Dutta A, Diao Y, Jain R, Rene ER, Dutta S. Adsorption of Cadmium from Aqueous Solutions onto Coffee Grounds and Wheat Straw: Equilibrium and Kinetic Study. J Environ Eng 2016;142:C4015014. doi: https://doi.org/10.1061/(asce)ee.1943-7870.0001015.
[46] Ho Y-S, McKay G. The kinetics of sorption of divalent metal ions onto sphagnum moss peat. Water Res 2000;34:735–42. doi: https://doi.org/10.1016/S0043-1354(99)00232-8.
[47] Putra EK, Pranowo R, Sunarso J, Indraswati N, Ismadji S. Performance of activated carbon and bentonite for adsorption of amoxicillin from wastewater: mechanisms, isotherms and kinetics. Water Res 2009;43:2419–30. doi: https://doi.org/10.1016/j.watres.2009.02.039.
[48] Lin Y, Xu S, Li J. Fast and highly efficient tetracyclines removal from environmental waters by graphene oxide functionalized magnetic particles. Chem Eng J 2013;225:679–85. doi: https://doi.org/10.1016/j.cej.2013.03.104.
[49] Akar E, Altinişik A, Seki Y. Using of activated carbon produced from spent tea leaves for the removal of malachite green from aqueous solution. Ecol Eng 2013;52:19–27. doi: https://doi.org/10.1016/j.ecoleng.2012.12.032.
[50] Anirudhan TS, Radhakrishnan PG. Thermodynamics and kinetics of adsorption of Cu(II) from aqueous solutions onto a new cation exchanger derived from tamarind fruit shell. J Chem Thermodyn 2008;40:702–9. doi: https://doi.org/10.1016/j.jct.2007.10.005.
[51] Banerjee P, Das P, Zaman A, Das P. Application of graphene oxide nanoplatelets for adsorption of Ibuprofen from aqueous solutions: Evaluation of process kinetics and thermodynamics. Process Saf Environ Prot 2016;101:45–53. doi: https://doi.org/10.1016/j.psep.2016.01.021.
[52] Weber WJ, Morris JC. Kinetics of adsorption on carbon from solution. J Sanitary Eng Div 1963;89:31–60.
[53] Khan AA, Singh R. Adsorption thermodynamics of carbofuran on Sn (IV) arsenosilicate in H^+, Na^+ and Ca^{2+} forms. Colloids Surf 1987;24:33–42. doi: https://doi.org/10.1016/0166-6622(87)80259-7.
[54] Liu Y, Liu Y-J. Biosorption isotherms, kinetics and thermodynamics. Sep Purif Technol 2008;61:229–42. doi: https://doi.org/10.1016/j.seppur.2007.10.002.
[55] Hu R, Wang X, Dai S, Shao D, Hayat T, Alsaedi A. Application of graphitic carbon nitride for the removal of Pb(II) and aniline from aqueous solutions. Chem Eng J 2015;260:469–77. doi: https://doi.org/10.1016/j.cej.2014.09.013.
[56] Ajmal M, Rao RAK, Anwar S, Ahmad J, Ahmad R. Adsorption studies on rice husk: removal and recovery of Cd (II) from wastewater. Bioresour Technol 2003;86:147–9. doi: https://doi.org/10.1016/S0960-8524(02)00159-1.
[57] Khani MH. Uranium biosorption by Padina sp. algae biomass: kinetics and thermodynamics. Environ Sci Pollut Res Int 2011;18:1593–605. doi: https://doi.org/10.1007/s11356-011-0518-0.
[58] Yao W, Yu S, Wang J, et al. Enhanced removal of methyl orange on calcined glycerol-modified nanocrystallined Mg/Al layered double hydroxides. Chem Eng J 2017;307:476–86. doi: https://doi.org/10.1016/j.cej.2016.08.117.
[59] Zhou L, Jin J, Liu Z, Liang X, Shang C. Adsorption of acid dyes from aqueous solutions by the ethylenediamine-modified magnetic chitosan nanoparticles. J Hazard Mater 2011;185:1045–52. doi: https://doi.org/10.1016/j.jhazmat.2010.10.012.
[60] Jin Z, Wang X, Sun Y, Ai Y, Wang X. Adsorption of 4-n-Nonylphenol and Bisphenol-A on Magnetic Reduced Graphene Oxides: A Combined Experimental and Theoretical Studies. Environ Sci Technol 2015;49:9168–75. doi: https://doi.org/10.1021/acs.est.5b02022.